Long exposure to extreme heat magnifies the decoupling between bacterial resistance and recovery

Ana-Hermina Ghenu[1], Anjaney J. Pandey[1,2,4], Zachary M. Bailey[1], David R. Johnson[1,3] and Madhav P. Thakur[1]

April 22, 2025

[1]Institute of Ecology and Evolution, University of Bern, Bern, Switzerland
[2]Department of Bioengineering, Indian Institute of Science, Bangalore, India
[3]Department of Environmental Microbiology, Swiss Federal Institute of Aquatic Science and Technology (Eawag), Dübendorf, Switzerland
[4]Undergraduate Programme, Indian Institute of Science, Bangalore, India

Authors' contributions. AHG: Conceptualization, Methodology, Software, Validation, Formal analysis, Investigation, Resources, Data Curation, Writing - Original Draft, Writing - Review & Editing, Visualization, Supervision, Project administration; **AJP:** Validation, Formal analysis, Investigation, Writing - Review & Editing; **ZMB:** Formal analysis, Investigation, Resources, Writing - Original Draft, Visualization; **DRJ:** Methodology, Writing - Review & Editing, Supervision; **MPT:** Conceptualization, Methodology, Writing - Original Draft, Writing - Review & Editing, Supervision, Project administration, Funding acquisition.

Funding. SNF project grant XXX awarded to MPT. ThinkSwiss Research Scholarship XXX awarded to AJP.

Acknowledgements. Members of the Terrestrial Ecology Division University of Bern, including Silvia Brochet (16S sequencing and species identification), Gerard Martínez-De León (stats discussion), Nicholas Tartini (stats discussion), and Anine Wiser (data collection). Chujin Ruan at Eawag (species interactions pilot experiment). Vladimir Senchillo at University of Lausanne (fluorescent strain construction).

Data accessibility. All data (except flow cytometry raw data) and complete analysis can be found at `https://github.com/EvoNerd/Xtreme_heat`. The flow cytometry raw data and analysis files can be found at `inserturlhere`

Subject area. Ecology, Microbiology, Environmental Science.

Keywords. climate change, soil microbes, community ecology

Corresponding author. AHG: ana.hermina.ghenu@gmail.com

Long exposure to extreme heat magnifies the decoupling between bacterial resistance and recovery

Abstract

Climate change is intensifying the duration of heat waves and threatening community stability. Using soil *Pseudomonas* communities, we investigated how different heat pulse durations impact resistance (immediate response) and recovery (post-stress response). We first assessed thermal performance traits across six species (16 strains) and found no trade-off between growth rate and heat resistance. We then assembled synthetic communities and exposed them to single heat pulses of 6, 12, 24, or 48 hours. We expected the fastest and most heat resistant species, *P. putida*, to dominate where present, but an intermediate grower, *P. protegens*, dominated all communities due to diffusible toxins and unexpected heat tolerance due to density-dependent growth. On average, each additional hour of heat increased extinction risk by 21.5% but fast growing communities were protected from extinction. The longest heat pulse duration led to sharp losses in diversity and productivity. We found that longer heat exposure magnified the decoupling between resistance and recovery phases, reducing community stability. These results reveal that growth rate and species interactions — not heat resistance alone — shape community fate during extreme events. Our findings highlight the need to consider nonlinear dynamics and trait-based interactions in predicting microbial responses to climate extremes.

1 Introduction

Climate change is driving more frequent, intense, and prolonged heat waves [1, 2]. These extreme events threaten biodiversity by increasing species extinctions, destabilizing communities, and disrupting ecosystem functioning [3, 4]. Yet, little is known about the ecological mechanisms that would destabilize communities during prolonged heat waves. Understanding how heat wave duration influences community dynamics is crucial for predicting these impacts. Moreover, identifying the mechanisms that determine community stability under such conditions can help predict which species are likely to persist or decline during climate extremes [5]. Using soil bacterial communities, we investigate species interactions and growth rates as core mechanisms shaping community stability in response to prolonged heat waves.

Trait based ecological approaches provide a promising way to understand the mechanisms of community stability and predict community responses to heat waves [6]. Modern coexistence theory proposes that a community's stability to perturbation depends on the life history strategies of its species [7]. Life history strategies are defined by the magnitude and co-variation of vital rates such as growth rate, stress resistance, and competitiveness. For example, slow growing species are typically excluded by fast growers unless there is a trade-off between growth rate and competitiveness. In this case, slow growing, competitive species can exclude others by promoting their own growth, limiting others, and resisting environmental stress. For example, plants with a slow life history strategy exhibit slow growth, high stress resistance, and high competitiveness [8]. We refer to this trend as the growth rate resistance trade-off. In order to better apply these findings to global change predictions, it is important to study these traits in a community context [9] and other taxa, such as bacteria [10].

Soil bacteria control up to 50–80% of the Earth's largest actively cycling reservoir of carbon, soil organic matter [11, 12]. These communities influence whether soils act as net sinks or sources of greenhouse gases [13, 14], so understanding the mechanisms of bacterial community stability under prolonged heat waves is crucial for improved climate change predictions. Similar to plants, bacteria are thought to exhibit a growth rate resistance trade-off, with slow growers faring better in extreme environments [15]. However, elevated temperature is a complex stressor [16] and very few studies have identified bacterial functional traits that are relevant for community stability during heat [17]. [18] and [19] found that growth rate and competitiveness tend to be negatively correlated in bacteria, leading to communities predictably being dominated by slow growing species at warmer

temperatures ($\leq 30°C$). There are very few studies that investigate the effect of increased heat pulse durations in this taxonomic group. Bacteria are ideal model organisms for testing general ecological principles because we can grow these communities in the laboratory at short timescales and high throughput.

In the laboratory, community stability [20] can be assayed experimentally by decomposing it into two phases: the immediate response to a stress event such as a heat pulse (resistance) and the response after the event subsides (recovery). A community's stability is estimated by measuring the extent of its response during the resistance and recovery phases as compared to an undisturbed control [21, 22]. Stable communities are expected to have a positive correlation, or coupling, between resistance and recovery [23, 24]. Coupling indicates that a community's short-term response can predict its long-term outcome [25–27]. In contrast, decoupling — a significant difference between resistance and recovery responses — indicates less predictability and suggests more complex dynamics, such as ecological trade-offs [4]. For example, increased decoupling of productivity in response to longer heat pulse duration was found in soil animals, where high survival investment during the resistance phase resulted in a trade-off with low fecundity during the recovery phase [28]. Bacteria are single-celled, meaning they cannot partition somatic versus gametic investment, so it is unknown whether bacterial communities can exhibit decoupling. Species richness is another ecological mechanism that impacts decoupling because diverse communities tend to have smaller total productivity responses during both resistance and recovery [29]. Assaying the presence and magnitude of decoupling using a resistance-recovery experimental framework will therefore link the short-term responses of bacterial communities to their long-term outcomes.

We conducted two interconnected experiments. The first (Experiment I) measured bacterial thermal performance traits to inform the second experiment (Experiment II), which used a resistance-recovery framework to examine the role of biotic interactions under varying heat pulse durations. In Experiment I, we screened six species (comprising 16 strains) of soil bacteria from the genus *Pseudomonas* for their bacterial traits at four high temperatures ($25, 30, 35$, and $40°C$). We hypothesized that bacterial species would exhibit a growth rate resistance trade-off. But we did not observe this. Although we could assign bacterial species to growth rate categories, the fastest grower, *P. putida*, was also the most heat resistant. Given this result, we set up Experiment II with four species on a gradient from fast to slow that retain the same rank order during heat (i.e., no trade-off between growth rate and heat resistance). The communities were inoculated at equal starting ratios in all 15 possible species combinations (i.e., singletons, pairs, triplets, and quadruplet), exposed to a single heat pulse of variable duration (6, 12, 24, or 48 hours (hrs)), then allowed to recover for a fixed two-day duration. We hypothesized that the fastest grower (*P. putida*) would dominate the communities exposed to the longer heat pulses, as it is also the most heat resistant. For all communities, we hypothesized that intrinsic growth rate and resistance to extreme heat, as measured from monocultures in Experiment I, would predict the composition and productivity of co-culture communities in Experiment II, with this effect becoming stronger with longer heat pulse duration.

2 Materials and methods

2.1 Medium and bacterial strains

LB broth (Lennox formulation) from Carl Roth was used throughout.

16 soil *Pseudomonas* strains from six species were used (Table S1) [30–34]. Samples were colony-PCR amplified, Sanger sequenced for 16S rRNA 27F/907R (corresponding to subregions V1-V5), and identified to the nearest species by BLASTN.

The four focal genotypes of Experiment II have constitutive expression of chromosomally integrated fluorescent proteins and were all built using an established gene delivery vector [35]. Fluorescent proteins were integrated onto the *P. putida* F1 (BSC001), *P. protegens* Pf5 (CK101), and *P. veronii* (BSC005) backgrounds in previous studies; the fluorescent genotype of *P. grimontii* (BSC028) [31] was built for this experiment using the Tn7 transposon delivery plasmid [35].

2.2 Experiment I

2.2.1 Thermal performance traits

For each strain, the probability of growth under heat stress was estimated by colony forming units (CFUs). Intrinsic growth rates and the intraspecific density dependence of growth rate were estimated using time-to-detection growth curves [36]. The time-to-detection approach allows estimation of density-independent (i.e., intrinsic) growth rates despite the high threshold of detection of the microplate reader [37].

The time-to-detection protocol was modified for high throughput by snap freezing the inocula into single-use 'shots', either at the stationary or early exponential phase. Bacteria were streaked on LB agar, incubated overnight at $28°C$, and single colonies were inoculated into liquid LB with 225 rpm shaking. For stationary phase inocula, 3.0 mL of media in culture tubes was incubated for 24 hrs, yielding an optical absorbance at 600 nm (OD_{600}) > 3. Then, cultures were resuspended to a final OD_{600} of 0.25 into their own filter-sterilized spent media with 10% glycerol. For early exponential phase inocula, 55 mL of LB in Erlenmeyer flasks was incubated to an OD_{600} between 0.01-0.05 ($\sim$ 4–7 hrs) and then resuspended into fresh media with glycerol as above. $100\mu L$ inocula were put in PCR strip-tubes and snap-frozen on dry ice. These single-use inoculum shots were stored at $-79°C$ and used within 2 months. Thawed inoculum shots were diluted into 900μL liquid LB to create a six-step, 10-fold dilution series (10^{-1} to 10^{-6}) that was used for CFUs and growth curves.

CFUs were incubated at three temperatures ($28°C$, $35°C$, and $40°C$) using the 6x6 drop plate method [38], with three replicates for each inocula culture phase. Using a P200 multichannel, droplets totaling 30μL of culture were plated onto 94mm LB agar petri dishes. Plates were incubated until colonies could be counted by eye (at least overnight) or failed to show discernible growth (at most 7 days).

Growth curves were run at four temperatures ($25°C$, $30°C$, $35°C$, and $40°C$) using 200μL cultures in 96-well microplates covered with a Breathe-Easy sealing membrane on Agilent BioTek Epoch 2 or Synergy H1 microplate readers with continuous double-orbital shaking at 807 cpm (1 mm) and a vertical heat gradient of $1°C$, to prevent condensation. OD_{600} was measured every 10 min [39] until cultures reached carrying capacity (at least 42 hrs) or failed to show discernible growth (at most 60 hrs). Replicate dilution series were done on three different days for each culture phase, randomizing the incubator and microplate well location.

2.3 Experiment II

2.3.1 Communities' resistance and recovery from extreme heat

As illustrated in Figure 1, bacterial communities were grown in a serial-transfer, batch culture system. Monocultures of *P. putida*, *P. protegens*, *P. grimontii*, and *P. veronii* were first inoculated from single colonies into Erlenmeyer flasks with 10mL 0.5x LB (Day -1) and incubated overnight as described above. The next morning (Day 0), the overnight monocultures were measured in triplicate by flow cytometry to determine their densities. After adjusting the density of each overnight monoculture, the four species were combined at equal cell densities into all 15 possible communities (n=5) and an estimated 10^3 cells were inoculated into 125μL of fresh media. The 15 communities were arranged in 5 blocks throughout the 96-well microplate (Figure S1) to randomize any edge effects [40]. The microplate was covered with parafilm and a lid to prevent differential evaporation at high temperature. Microplates were incubated in Agilent Epoch 2 or Synergy H1 readers with continuous double-orbital shaking at 205 cpm (5 mm) for a day (22–23 hrs) and OD_{600} was acquired regularly throughout. Each day (Days 1–5), 5% of the culture was transferred to fresh media and the remainder was measured by flow cytometry to estimate species abundances.

2.3.2 Estimating species abundances by flow cytometry & identifying extinctions

Cell counts were recorded using an Invitrogen Attune CytPix flow cytometer with blue/violet/yellow lasers, NxT Fluorescent Protein Filter Kit, NxT Small Particle Side-Scatter Filter, and CytKick autosampler. Cultures were diluted in 7.52 mM tetrasodium pyrophosphate at pH 7.5 to a concentration of 10^{-3}x for overnight monocultures (Day 0) or 10^{-2}x for community inocula (Day 0)

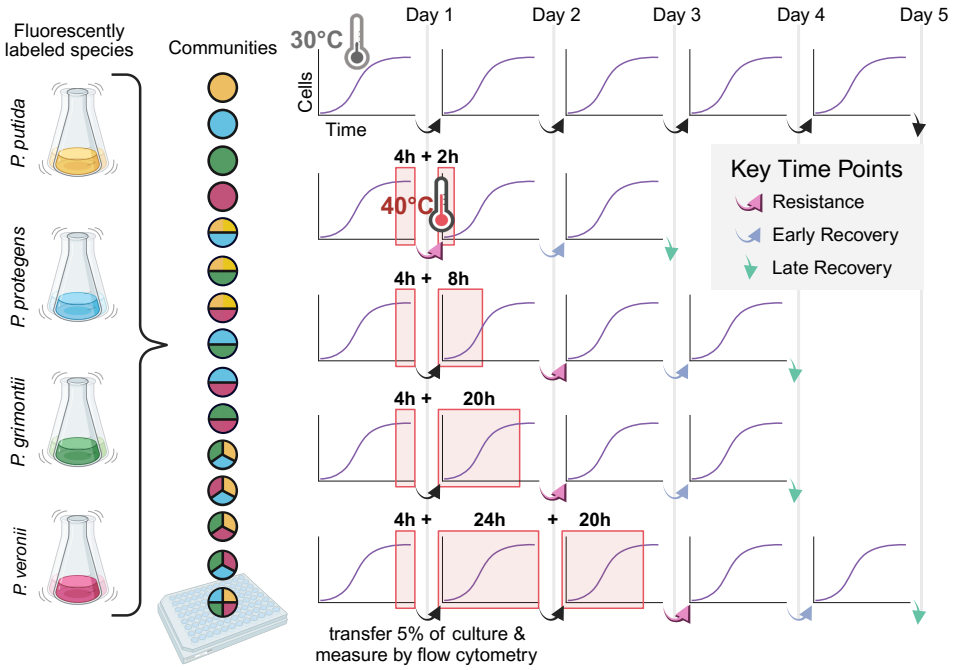

Figure 1: **Design of resistance and recovery experiment with variable heat pulse duration.** Overnight monocultures of four species constitutively expressing fluorescent proteins (flasks at left) were inoculated at equal ratios in all 15 combinations of communities (coloured circles) into a 96-well microplate. Batch cultures were measured for their species abundances by flow cytometry and transferred daily (arrows). Starting from the end of Day 1, the cultures were exposed to a single $40°C$ heat pulse of variable duration (6, 12, 24, or 48 hrs; highlighted in red) then allowed to recover for two days. Measurements near the end of or just after the heat pulse are referred to as 'resistance' time points (bold pink arrow), while those from the first or second day post-heat are called early or late recovery (purple-blue and turquoise arrows), respectively. Treatments are always compared with the no-heat control on the same day of serial transfer. Figure made with BioRender.

and serially-transferred communities (Days 1-5). Bacterial cells were separated from debris using a rectangular gate in side-scatter area and forward-scatter area. Up to 10^4 events in the bacterial cells gate were sampled from up to 146μL of diluted cultures at 25μL/min.

Cell counts and well volumes were extracted from the flow cytometry data using FCS Express (version 7.22.0006) and the Attune Cytometric Software (version 6.1.1), respectively, to estimate event densities. Events from the bacterial cell gate were classified into four fluorophore-specific subsets using four sets of three nested polygonal gates in the fluorescent channel heights (these gates were also used to exclude doublets). As each species expresses a unique fluorophore, this allowed us to estimate species-specific cell counts by identifying singlet cells that express only the appropriate fluorophore. Absolute species abundances were estimated by dividing the flow cytometry cell counts by the acquired well volume.

The threshold of detection of the flow cytometer is operationally defined as 50 events in the bacterial cell gate, which is more than twice the maximum number of events that we recorded for a true blank.

The serial-transfer OD_{600} data was used to estimate the rate of contamination and to verify extinction events. Contamination was inferred to have occurred in well blanks when a baseline-subtracted $OD_{600} > 1$ was detected at any time. Extinction was inferred to have occurred for community replicates where the baseline-subtracted OD_{600} on the last day of recovery never surpassed the maximum value for uncontaminated well blanks. Extinction events were confirmed by flow cytometer cell counts below the threshold of detection.

2.3.3 Assaying diffusible species interactions

P. protegens, *P. putida*, *P. grimontii*, and *P. veronii* (hereafter the focal species) were grown in co-cultures with *P. protegens* in 25 mL flasks for 24 hours at 220 rpm and $30°C$. These cultures were centrifuged at 10 000 g for five minutes, the supernatant was removed, filtered twice using a 0.22 μm PES filter, and plated to preclude live bacteria. This supernatant was mixed with fresh media and aliquoted to 96-well microplates so that each focal species could be subjected to 90%, 80%, 70%, 60%, 50%, 40%, 30%, 20%,10% ,5%, and 0% of each supernatant. The OD_{600} of each population was measured over 12 hrs with a BioTek plate reader. The final versus initial OD_{600} was compared to determine the effect of diffusible secondary metabolites produced by *P. protegens* on focal species' growth. The inhibitory concentration where the population is reduced by 50% (IC_{50}) was estimated for each focal species by nonlinear least squares fitting using the nlsLM function (minpack.lm [41]) with a Hill curve equation and being self-started with.

2.4 Statistical analyses

All statistical analyses were performed in R (version 4.4.2 [42]) and the code for analysis of both experiments is provided in the supplementary material and GitHub repository.

For Experiment I, the growth rates were estimated from the interpolated baseline-subtracted optical absorbance data in the mid-exponential phase (time-to-detection threshold $OD_{600} = 0.05$), the estimated inoculum size from CFUs, and calibration curves for each microplate reader [43]. Intraspecific density dependence was estimated as per-capita derivatives from gcplyr (version 1.10.0 [44]). To test for a correlation between the growth rates at ambient temperatures ($25°C$ or $30°C$) with the species' growth traits (intrinsic growth rate or probability of growth by CFU) at extreme heat ($40°C$), we used both a parametric approach with linear mixed models as well as a non-parametric approach with the species rankings.

For Experiment II, species abundances were analyzed at three key time points (Figure 1): 'resistance' (last day of the heat pulse), 'early recovery' (first day post-heat), and 'late recovery' (second day post-heat). Ordination analysis by non-metric multidimensional scaling (NMDS; vegan, version 2.6.8 [45]) was performed to summarize the overall effect of heat duration over time across the different communities. For no-heat control communities, measurements were used from Days 1, 3, and 5. As each community contained only one to four species, species abundances at the three key time points were treated as variables (i.e., columns) and each replicate was treated as a unique observation (i.e., rows) in the abundance matrix. Distances were calculated using the Bray-Curtis dissimilarity. Heat pulse duration was fitted as an environmental vector onto the ordination using the envfit function (vegan).

Effect sizes on Shannon diversity and total productivity as compared to no-heat control were estimated in Experiment II by fitting separate generalized linear models (GLMs) for each heat duration treatment and its corresponding key time point control. For each heat duration, diversity and productivity during resistance, early recovery, and late recovery were compared to the corresponding control data from the same days (e.g., days 1–3 for 6 hrs, days 3–6 for 48 hrs heat pulse; Figure 1). The full data was rescaled by its standard deviation, fitted to GLM families with different link functions (glmmTMB, version 1.1.11, [46]) that were compared by simulating their residuals (DHARMa, version 0.4.7, [47]), and the best fitting family of distributions was chosen. A lognormal or Poisson family of distributions was chosen when diversity or productivity, respectively, were used as response variables. As our data contained zero values, but the lognormal distribution does not allow zero values, we transformed the diversity data by adding a small value to all our data points ($\epsilon = \frac{\text{smallest non-zero value}}{100}$). Then, the data was divided into four subsets for each heat duration with its corresponding no-heat control at the appropriate key time points, checked for predictor multicollinearity (performance, version 0.12.4, [48]), and fitted to different models. The overall best model was selected by averaging the values of the Akaike and Bayesian information criteria (AIC and BIC, respectively) across the four data subsets. The base model had an interaction between Heat * Treatment Day. The inoculated community richness was included in the base model when the response variable was diversity and it was included in the alternative models when the response variable was productivity. Alternative models had combinations of three additional predictors: the presence/absence of the heat resistant species *P. putida*, the pres-

ence/absence of the strong competitor species *P. protegens*, and the expected community growth rate. The expected growth rate was estimated for each community by averaging the intrinsic growth rates of the species inoculated in that community. Effect sizes were estimated as compared to the no-heat control (effsize, version 0.8.1, [49]), then the estimated marginal means (emmeans, version 1.10.5, [50]) were used to summarize the overall effect of heat duration on resistance, early recovery, and late recovery days. For numeric non-focal predictors (inoculated community richness and community expected growth rate), this was done by using their mean values. For categorical non-focal predictors (presence/absence of a strong competitor), this was done by marginalizing over the predictor levels. Finally, pairwise t-tests with Bonferroni-corrected ($\alpha = 10^{-3}$) were used to compare different heat duration treatments.

3 Results

3.1 Experiment I

3.1.1 Congeneric species exhibit consistent growth rate rankings across temperatures

We screened the growth rate of six soil *Pseudomonas* species (in total 16 genotypes, listed in Table S1) at four temperatures, with cultures inoculated either from early exponential phase (Figure 2A) or stationary phase (Figure S2). The rank order of the species median growth rates was weakly positively correlated across temperatures (Kendall's coefficient of concordance, Wt=0.75, $\mathcal{X}^2$=11.2, df=5, p¡0.05). Except for two, most species had a consistent ranking across different temperatures.

3.1.2 Growth rates are not correlated with extreme heat resistance

To determine which of the two elevated temperatures ($35°C$ or $40°C$) constitutes a heat extreme, we assessed whether the net growth rate was substantially reduced across all species, indicating conditions severe enough to prevent cell proliferation or even induce cell mortality. Using a two-sided Wilcoxon signed rank test, we found that CFUs at $40°C$ were consistently lower than those at $35°C$ (V=$4.16 \cdot 10^3$, p< 10^{-10}), regardless of the species or growth phase of the inoculum. Figure 2B shows the CFU of cultures incubated at high temperatures relative to their CFU at the average temperature these bacteria are usually cultured at in the lab ($28°C$) for early exponential phase inocula (see Figure S3 for stationary phase inocula). Most species exhibited no growth at $40°C$ (Figure 2B). Across all species and inocula, the relative fraction of CFUs directly predicted the fraction of batch cultures with binary presence or absence of growth (all temperatures: $\beta = 0.81$, p< 10^{-10}; $40°C$: $\beta = 0.88$, p< 10^{-10}), resulting in consistent growth estimates between the batch culture data from liquid media and the CFU data from solid media (linear regression, $30°C$: $R^2 = 0.84$, F(1, 94)=508, p< 10^{-10}; $40°C$: $R^2 = 0.80$, F(1, 30)=126, p< 10^{-10}). A paired samples t-test also showed that the intrinsic growth rates were significantly lower at $40°C$ than at $35°C$ for the batch culture data (t(31)=11.5, p< 10^{-10}). Therefore, we conclude that $40°C$ can be considered hot enough to be an extreme heat temperature that consistently impairs the growth of soil bacteria in our experiment.

Finally, we tested the hypothesis for Experiment I that slow growers are more resistant to extreme heat. For all analyses, we failed to reject the null hypothesis of no correlation between a species' growth rate at ambient temperatures and its ability to resist extreme heat (Tables S2-S4). There was no support for a growth rate resistance trade-off.

3.2 Experiment II

For Experiment II, we selected four species (solid lines in Figure 2A) whose rank order is unchanged across temperatures (Wt=0.90, $\mathcal{X}^2$=8.08, df=3, p¡0.05).

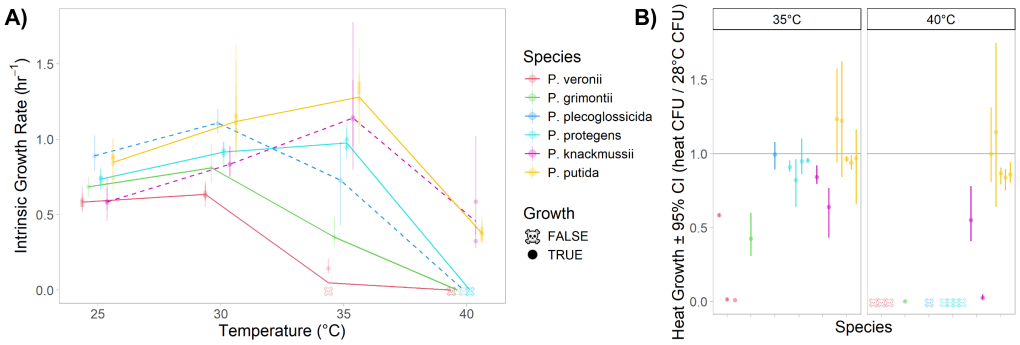

Figure 2: **Net growth rate as a function of temperature (i.e., thermal performance curves) for six bacterial species, in liquid and solid media. A)** Batch-culture intrinsic net growth rates (points) ± bootstrapped 95% confidence intervals (error bars) are shown for each strain inoculated from early exponential phase. Temperatures without consistent growth after 48hrs are shown as skulls. Lines connect species averages, with solid lines indicating species with consistent rank across temperatures (used in Experiment II) and dashed lines indicating species that change rank across temperatures. **B)** CFUs at stress temperature as a fraction of CFUs at $28°C$ (dots) ± bootstrapped 95% confidence intervals (error bars) are shown for each strain inoculated from early exponential phase. Temperatures without any growth after 7 days are shown as skulls.

3.2.1 *P. protegens* is a strong competitor that dominates all the communities where it was inoculated

The second fastest-growing species, *P. protegens*, dominated all communities in which it was inoculated irrespective of heat treatment. This pattern is evident in the ordination plot (Figure 3A), which illustrates community trajectories over time across the resistance, early recovery, and late recovery (see Key Time Points in Figure 1). An NMDS with three dimensions was found to summarize much of the variation in the data (stress=0.0565; Figure S6). The ordination revealed a clear separation between communities containing *P. protegens* and those without *P. protegens*. NMDS clusters indicate a significant interaction between the presence of *P. protegens* and heat pulse duration, as confirmed by non-parametric bootstrapping (ANOSIM, R statistic = 0.621, p ¡ 0.001).

All multi-species communities inoculated with *P. protegens* lost their species richness within one day, regardless of heat (Figure 3B). The multi-species communities that were not inoculated with *P. protegens* managed to maintain at least some of their species richness over time. However, for these communities, species richness was lost as heat pulse duration increased.

We found that supernatant from *P. protegens* co-cultures has a strong inhibitory effect not seen in monoculture supernatant (Figure S7). Supernatant experiments show that *P. protegens* has inducible expression of diffusible metabolites at $30°C$ that effectively inhibit the growth of the other species (Figure 3C).

3.2.2 Fast growing communities are protected from extinction

The NMDS ordination (Figure 3A) also reveals a trend of longer heat pulse durations generally shifting community positions downward, with the exception of the longest heat pulse duration (48 hrs). This environmental gradient is not statistically significant when the 48 hr heat pulse duration is included (p = 0.30) or when it is excluded entirely (stress = 0.0359; p = 0.22). However, the gradient becomes significant when communities subjected to the 48 hr heat pulse in the absence of *P. protegens* are excluded (Figure S8; stress = 0.0370; p ¡ 0.001). What is it that makes the 48 hr heat pulse duration in the absence of *P. protegens* different than the other communities and heat treatments?

A logistic regression model (Figure S9) explained about 70.7% of the variation (by Efron's pseudo r-squared) in the extinction data. It had an additive effect of heat pulse duration, the presence of *P. protegens*, and expected community growth rate. Contrary to our hypothesis, this

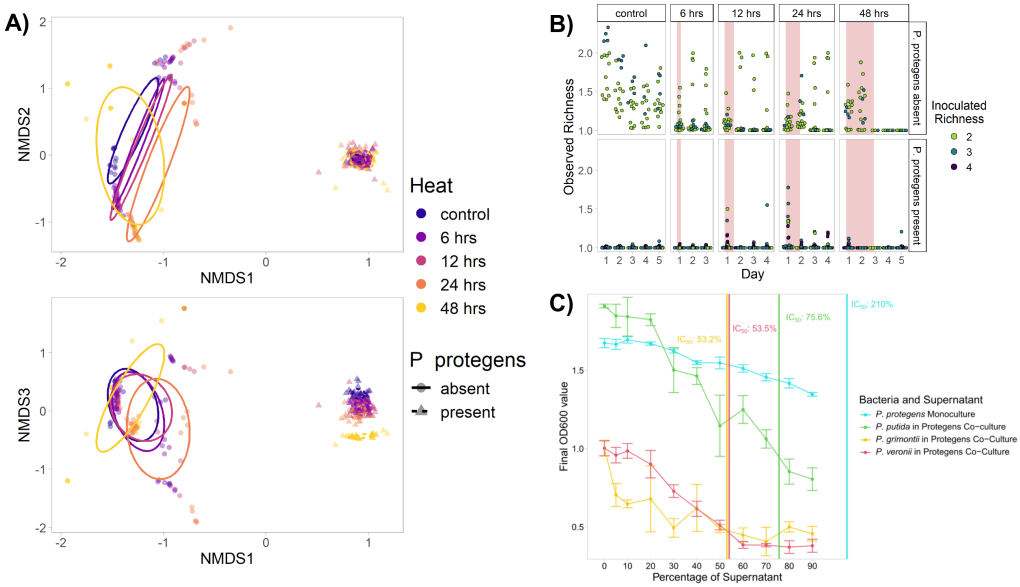

Figure 3: ***P. protegens* dominates all communities where it was inoculated because it is an effective killer. A)** Ordination plot of NMDS axes 1 versus 2 (top) and axes 1 versus 3 (bottom) shows that the presence (triangles and dashed-line ellipses) or absence (circles and solid-line ellipses) of *P. protegens* explains much of the variation in the data. The remaining variation in the data is explained by increasing heat pulse duration (warmer colours). The points show the different communities over time and the ellipses show the standard error of the (weighted) average of scores. **B) Communities without *P. protegens* (top row) and with a short duration (or no) heat pulse (left columns) are able to maintain more of their inoculated community richness** than communities with *P. protegens* (bottom row) or with a long duration heat pulse (right columns). Points show the first-order Hill diversity index, which approximates the species richness while allowing for flow cytometry noise. The red background colour indicates days when the $40°C$ heat pulse was administered. **C) *P. protegens* expresses diffusible metabolites that effectively inhibit the growth of other bacterial species.** The presence of increasing supernatant concentration (x-axis) from *P. protegens* co-cultures has a negative effect on the final OD_{600} (y-axis). Vertical lines indicate the estimated supernatant concentration where the population's growth is inhibited by 50% (IC_{50}).

model was preferred over one where the presence of the heat resistant species *P. putida* was included as a predictor (ΔBIC = 48.1).

The logistic regression estimated that communities where *P. protegens* had been inoculated were less likely to go extinct. However, this estimate (odds: $2.71 \cdot 10^{-11}$, 95% CI: $[0, \infty)$, p=0.999) is unreliable, likely because we never observed a single extinction for these communities even for the 48 hr heat pulse duration (n=35). In contrast, six extinction events (n=35) were observed for communities inoculated with the heat resistant *P. putida*, the species that was identified in Experiment I as growing reliably at $40°C$. If we look more closely at the growth curve data from Experiment I, we see that *P. protegens* exhibited a density-dependence in its ability to grow under extreme heat. The highest inoculum concentration at $40°C$ had a similar time to detection as for lower temperatures but all other inoculum concentrations failed to grow at this extreme heat (Figure S4). A similar result was also observed for colonies on solid media (data not shown). Unlike the other species, *P. protegens* exhibits a positive density-dependence of growth rate even at an ambient temperature (Figure S5).

Fast-growing communities were more protected from extinction. The odds of extinction increased by 21.5% (95% CI: [0.111, 0.319]) for each additional hour of heat pulse duration. On the other hand, communities with faster growth rates were $2.26 \cdot 10^6$ times more likely (95% CI: $[120, 4.27 \cdot 10^{10}]$) to survive for each unit of growth rate increase. In conclusion, communities with faster-growth rates and those inoculated with *P. protegens* were protected from the extinction that

was caused by longer heat pulse durations.

3.2.3 Long duration heat pulse magnifies the decoupling between resistance and recovery

To gauge how community stability changed with increasing heat pulse duration, we estimated decoupling for Shannon diversity and total productivity.

For diversity, the model that best fit the data was a complex model with 25 parameters: an additive effect of inoculated community richness; and a four-way interaction between the heat pulse duration, treatment day, presence/absence of *P. protegens*, and community expected growth rate. As this model was too complex to interpret, we chose to investigate the second best model (ΔBIC = 8.32), which had 16 parameters: an additive effect of inoculated community richness; a three-way interaction between the heat pulse duration, treatment day, and presence/absence of *P. protegens*; and an interaction between the presence/absence of *P. protegens* and community expected growth rate. Contrary to our hypothesis, models with the presence/absence of the heat resistant species *P. putida* fit poorly (ΔBIC $\geq$ 163). All heat pulse durations led to a significant loss of biodiversity that never recovered, even two days after the heat pulse ended (Figure S10). The loss of biodiversity was significantly greater for the 48 hr heat pulse (Table S5). The results remained consistent even after excluding extinct communities (Figure 4A). No decoupling was observed.

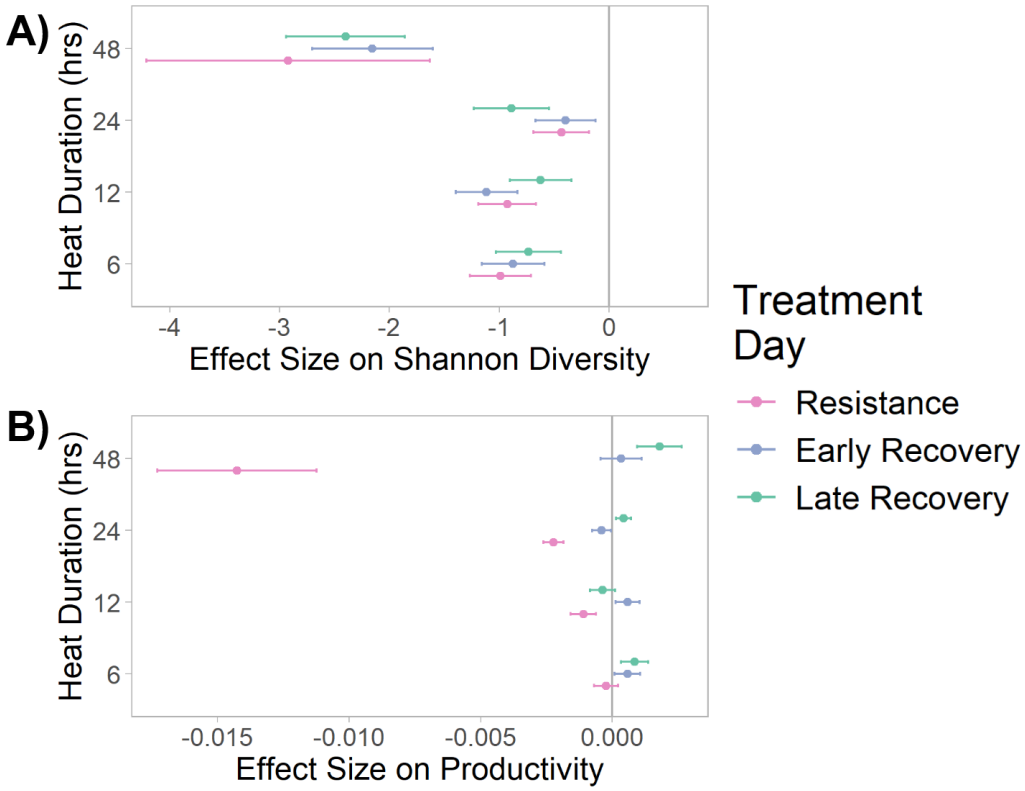

Figure 4: **Different metrics show larger effect sizes for the longest heat pulse event, 48h.** Forest plots show the estimated effect sizes and their 95% confidence intervals from generalized linear models. All communities that experienced extinction have been excluded from the data. **A)** The response variable is Shannon diversity as estimated from flow cytometry absolute cell densities for each of up to four species. **B)** The response variable is productivity as estimated from flow cytometry absolute cell density summed across all species present in the community.

The model that best fit the productivity data was a complex model (26 parameters), similar to the best fitting one for biodiversity. We chose to investigate the second best model as its fit was indistinguishable (ΔBIC = 1.04). This simpler model had 16 parameters: an additive effect

of community expected growth rate; a three-way interaction between the heat pulse duration, treatment day, and presence/absence of *P. protegens*; and an interaction between presence/absence of *P. protegens* and inoculated community richness. Contrary to our hypothesis, models with the presence/absence of the heat resistant species *P. putida* fit poorly (ΔBIC $\geq$ 188).

We found that longer heat durations led to larger, negative effects during resistance, especially for the longest heat pulse duration of 48 hrs (Figure S11, Table S6). We found that decoupling between resistance and recovery (both early and late) seemed to increase somewhat with heat duration (Figure S12). Extinct wells, by definition, were not able to recover and therefore were perfectly coupled. To assess whether the increased extinction risk associated with longer heat pulse durations influenced our results, we excluded all communities that experienced extinction, repeated the analysis, and observed consistent results (Figure 4B). After excluding extinct communities, long heat pulse events were found to lead to slightly positive effects during recovery. A sharp increase in decoupling was observed for the 48 hr heat pulse duration (Figure 5).

4 Discussion

Our study aimed to identify the ecological mechanisms that shape soil bacterial community stability under varying heat pulse durations. We sought to predict bacterial community responses from species growth rate and heat resistance. By estimating thermal performance traits for six congeneric species (comprising 16 strains; Experiment I), we found no support for the hypothesized trade-off between growth rate and resistance. Although species exhibited fairly consistent growth rate rankings across temperatures, these were uncorrelated with resistance to extreme heat. For the heat pulse duration experiment (Experiment II), we selected four species with variable growth rates and hypothesized that the fastest and most heat resistant species, *P. putida*, would dominate all the communities where it was inoculated. Surprisingly, an intermediate grower, *P. protegens*, out-competed all the other species, regardless of heat, because it was an effective killer. In addition, *P. protegens* was resistant to even the longest heat pulse duration, although the thermal performance screen identified it as heat sensitive. On average, longer heat pulses drove communities to extinction. Each additional hour of heat exposure increased the odds of community extinction by 21.5%, but communities with faster growing species were substantially protected ($\sim 10^6$ times more likely to survive). Even among communities that evaded extinction, community stability decreased nonlinearly with increased heat pulse duration. Both species diversity and total productivity declined during the shorter heat pulses (6–12 hrs), then fell sharply during the longest heat pulse. The longest heat duration caused a sharp decoupling in total productivity responses during versus after the pulse, indicating reduced community stability. In summary, our study suggests that growth rates are a key factor in community stability against prolonged heat waves. However, specific species interactions can override the predictions from monoculture traits and significantly alter the community outcomes.

In Experiment I, we found variation in thermal performance traits among closely related species, indicating diverse growth strategies and heat resistances. The strains used here are primarily natural isolates and likely represent the diversity of thermal strategies adopted by soil *Pseudomonads*. Although *Pseudomonads* are broadly considered mesophiles [51], fine grain thermal niches may distinguish species. The greater between-species than within-species differences in thermal niche could suggest that this represents an important species difference in *Pseudomonads*, as recently found in Eukaryotic microbes [52]. The mixture of thermal niches and growth strategies observed here likely reflects the spatial and temporal heterogeneity of soil [53–55], which supports exceptionally high microbial biodiversity [56].

Contrary to our expectation from the monoculture experiments, the intermediate grower *P. protegens* dominated all communities where it was inoculated in Experiment II and never experienced extinction. Follow-up supernatant experiments and closer examination of the growth curve OD_{600} data showed that this species is competitive because it can produce diffusible metabolites, and facilitate its own growth even during extreme heat. Although the OD_{600} data at $25°C$ could be explained by cellular changes in size or aggregation, those at $40°C$ are clearly indicative of density-dependent survival or growth facilitation under stress. Our findings reinforce that monoculture-based traits, such as growth rates, cannot solely predict community dynamics, a con-

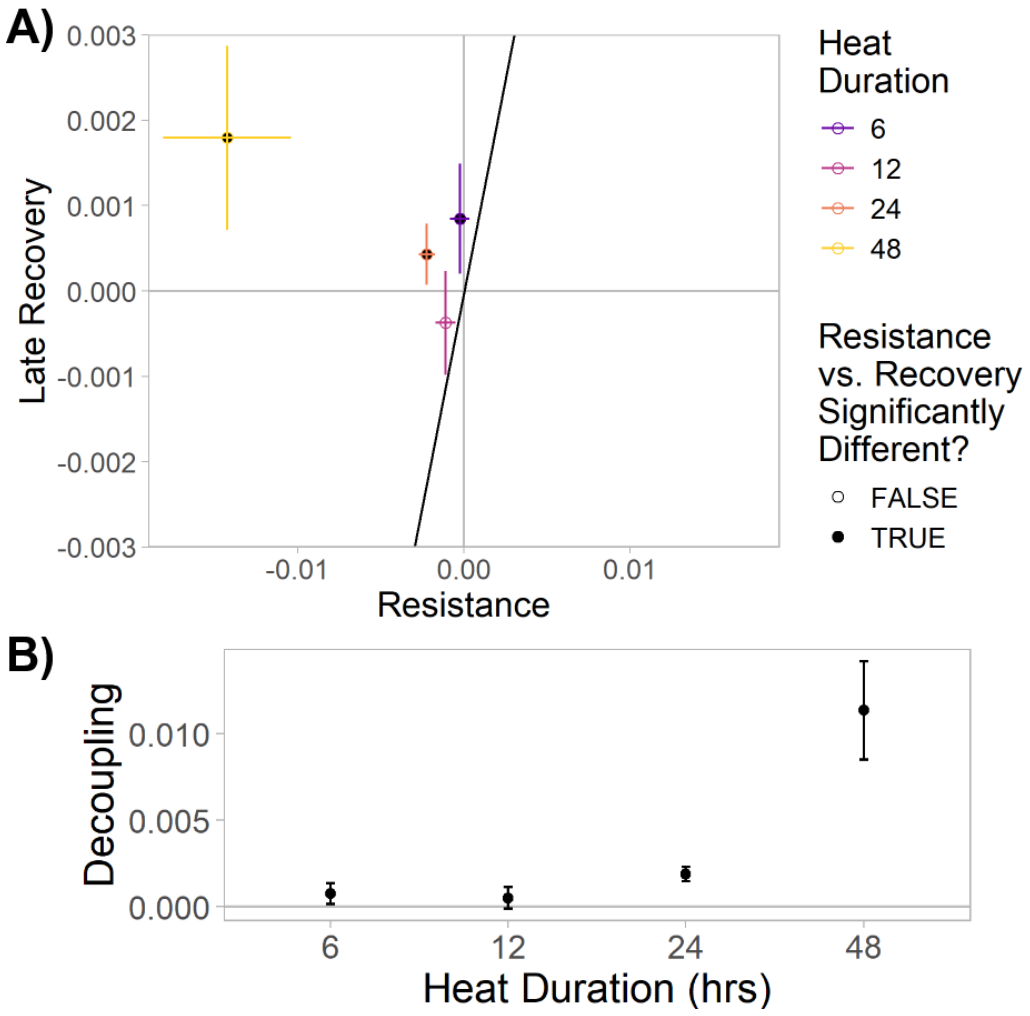

Figure 5: **Productivity exhibited decoupling of resistance from recovery, especially for the longest heat pulse duration (48h). A)** The x-axis shows the effect size on the resistance treatment day, the y-axis shows the effect size on the late recovery treatment day, and the black diagonal line indicates y=x. The coloured points show the mean estimate for different heat pulse durations and the cross-hairs indicate their univariate 95% confidence intervals. Decoupling occurs when the effect size of resistance is significantly different from that of recovery; these statistically significant points are filled with black. **B) Decoupling increases sharply for long heat pulse durations.** Mean estimated decoupling (points) is plotted directly from the panel above by measuring the shortest Euclidean distance between the point estimate and the y=x line. The lines show the confidence intervals that were estimated by drawing ovals around the univariate confidence intervals then measuring the shortest and longest Euclidean distance between the oval and the y=x line. All communities that experienced extinction have been excluded from the data.

clusion supported by previous work [37, 57, 58]. Supernatant experiments can effectively assess species interactions but may be misleading when toxin expression is inducible [59, 60]. *P. protegens* toxicity aligns with previous studies identifying it as a biocontrol agent [61] capable of excluding other soil bacteria, including other *Pseudomonads* [62], by antibiotic secretion [63] and contact-dependent killing [64]. Future studies should investigate the mode of action of *P. protegens'* toxicity under different environmental variables relevant to climate change and in the community context [6, 9]. Finally, our work demonstrates that the time-to-detection method [36] can be used to estimate density-dependent effects. This suggests that high-throughput monoculture growth experiments can be better leveraged to estimate species functional traits [37].

Our understanding of bacterial functional traits that influence life history strategies and com-

munity dynamics is limited as compared to other taxa. In plants, for example, functional traits such as specific leaf area, seed size, and wood density are well established as indicators of life history strategies [8]. In bacteria, the most well characterized functional trait is ribosomal RNA operon copy number, which correlates with maximum growth rate [65, 66]. However, comprehensive trait frameworks are still missing. While other studies have explored various bacterial functional traits [10, 67–69], including those related to heat resistance [17], these findings focus on distant phylogenetic relationships. Using a trait-based methodology for predicting interactions remains a challenge, especially for closely related species, as in our study. Our research suggests that density dependence in growth rate may serve as a valuable trait for predicting resistance and interactions between closely related bacteria. Future studies should systematically investigate density dependence further to determine if it correlates with life history strategies such as stress resistance and competitive ability.

The main contribution of this work is the finding that decoupling between resistance and recovery increases nonlinearly in bacterial communities due to prolonged heat pulse duration. In our study, this decoupling is driven by the positive selection of species with higher growth rate and heat resistance. The prolonged 48 hr heat pulse restructured community composition through loss of slower growing species. Communities composed of only slow growing species were unable to recover and went extinct, exhibiting a perfect coupling between resistance and recovery. In contrast, communities that escaped extinction were enriched with fast growing, heat resistant species, which showed over recovery. Consequently, the communities that survived extinction displayed a strong decoupling due to the intense negative response during resistance and mild positive response during recovery (Figure 5). Notably, our findings provide a new mechanism for decoupling [4] that is distinct from the trade-off between survival and fecundity that is commonly seen in multicellular organisms [70], including soil invertebrates exposed to heat [28]. While survival fecundity trade-offs can be identified by their positive response (high survival) during resistance and negative (low fecundity) one during recovery [28], the mechanism of decoupling that we describe here has an opposite pattern. This decoupling is caused by a positive correlation between growth rate and heat resistance in soil *Pseudomonads*, suggesting that species or stressors that elicit a growth rate resistance trade-off may elicit different patterns of decoupling. Future studies should examine decoupling in other microbial taxa and other environmental stressors to determine if our findings are generalizable.

In contrast to a previous meta-analysis that found no evidence of a threshold effect for many types of anthropogenic global change stressors [71], our study finds nonlinear responses for prolonged heat duration. We expect this threshold effect of heat duration to be generalizable to both Eukaryotic and natural communities because it is caused by increased extinction risk with increased heat wave duration. Extinction is a local equilibrium for most ecological systems. Future studies should look at the threshold effect of heat wave duration.

5 Conclusion

Longer heat wave durations have a nonlinear impact on bacterial communities, significantly increasing the risk of extinction for slower growing species. Even communities that avoid extinction are likely to be destabilized, as indicated by a larger decoupling between their responses during resistance and recovery. This suggests that prolonged heat waves reshape the composition and reduce the stability of communities, particularly affecting interactions among different growth rate strategies.

Ethics. This work did not require ethical approval from a human subject or animal welfare committee.

Declaration of AI use. The writing of this manuscript was aided by use of DeepAI and ChatGPT for editorial purposes. After using these tools, the authors reviewed and revised all text as needed. We therefore assume full responsibility for the content of this document.

Conflict of interest declaration. We declare no conflict of interest.

References

[1] Domeisen DIV, Eltahir EAB, Fischer EM, Knutti R, Perkins-Kirkpatrick SE, Schär C, Seneviratne SI, Weisheimer A, Wernli H. 2023 Prediction and projection of heatwaves. *Nature Reviews Earth & Environment* **4**, 36–50.

[2] IPCC. 2023 Summary for Policymakers. In Core Writing Team, Lee H, Romero J, editors, *Climate change 2023: Synthesis report. Contribution of working groups I, II and III to the sixth assessment report of the Intergovernmental Panel on Climate Change* , pp. 1–34. Geneva, Switzerland.

[3] Harvey JA, Heinen R, Gols R, Thakur MP. 2020 Climate change-mediated temperature extremes and insects: from outbreaks to breakdowns. *Global change biology* **26**, 6685–6701.

[4] Martínez-De León G, Thakur MP. 2024 Ecological debts induced by heat extremes. *Trends in ecology & evolution*.

[5] Pacifici M, Foden WB, Visconti P, Watson JE, Butchart SH, Kovacs KM, Scheffers BR, Hole DG, Martin TG, Akçakaya HR et al.. 2015 Assessing species vulnerability to climate change. *Nature climate change* **5**, 215–224.

[6] de Bello F, Lavorel S, Hallett LM, Valencia E, Garnier E, Roscher C, Conti L, Galland T, Goberna M, Májeková M et al.. 2021 Functional trait effects on ecosystem stability: assembling the jigsaw puzzle. *Trends in Ecology & Evolution* **36**, 822–836.

[7] Barabás G, D'Andrea R, Stump SM. 2018 Chesson's coexistence theory. *Ecological monographs* **88**, 277–303.

[8] Adler PB, Salguero-Gómez R, Compagnoni A, Hsu JS, Ray-Mukherjee J, Mbeau-Ache C, Franco M. 2014 Functional traits explain variation in plant life history strategies. *Proceedings of the National Academy of Sciences* **111**, 740–745.

[9] Stillman JH. 2019 Heat waves, the new normal: summertime temperature extremes will impact animals, ecosystems, and human communities. *Physiology* **34**, 86–100.

[10] Martiny JBH, Jones SE, Lennon JT, Martiny AC. 2015 Microbiomes in light of traits: a phylogenetic perspective. *Science* **350**, aac9323.

[11] Crowther TW, Van den Hoogen J, Wan J, Mayes MA, Keiser A, Mo L, Averill C, Maynard DS. 2019 The global soil community and its influence on biogeochemistry. *Science* **365**, eaav0550.

[12] Whalen ED, Grandy AS, Sokol NW, Keiluweit M, Ernakovich J, Smith RG, Frey SD. 2022 Clarifying the evidence for microbial-and plant-derived soil organic matter, and the path toward a more quantitative understanding. *Global Change Biology* **28**, 7167–7185.

[13] Liang C, Schimel JP, Jastrow JD. 2017 The importance of anabolism in microbial control over soil carbon storage. *Nature microbiology* **2**, 1–6.

[14] Glassman SI, Weihe C, Li J, Albright MBN, Looby CI, Martiny AC, Treseder KK, Allison SD, Martiny JBH. 2018 Decomposition responses to climate depend on microbial community composition. *Proceedings of the National Academy of Sciences* **115**, 11994–11999.

[15] Gilbert P, Collier PJ, Brown MR. 1990 Influence of growth rate on susceptibility to antimicrobial agents: biofilms, cell cycle, dormancy, and stringent response. *Antimicrobial agents and chemotherapy* **34**, 1865–1868.

[16] Litchman E, Edwards KF, Klausmeier CA. 2015 Microbial resource utilization traits and trade-offs: implications for community structure, functioning, and biogeochemical impacts at present and in the future. *Frontiers in microbiology* **6**, 254.

[17] Knight CG, Nicolitch O, Griffiths RI, Goodall T, Jones B, Weser C, Langridge H, Davison J, Dellavalle A, Eisenhauer N et al.. 2024 Soil microbiomes show consistent and predictable responses to extreme events. *Nature* pp. 1–7.

[18] Lax S, Abreu CI, Gore J. 2020 Higher temperatures generically favour slower-growing bacterial species in multispecies communities. *Nature ecology & evolution* **4**, 560–567.

[19] Abreu CI, Dal Bello M, Bunse C, Pinhassi J, Gore J. 2023 Warmer temperatures favor slower-growing bacteria in natural marine communities. *Science Advances* **9**, eade8352.

[20] Donohue I, Petchey OL, Montoya JM, Jackson AL, McNally L, Viana M, Healy K, Lurgi M, O'Connor NE, Emmerson MC. 2013 On the dimensionality of ecological stability. *Ecology letters* **16**, 421–429.

[21] Neubert MG, Caswell H. 1997 Alternatives to resilience for measuring the responses of ecological systems to perturbations. *Ecology* **78**, 653–665.

[22] Kéfi S, Domínguez-García V, Donohue I, Fontaine C, Thébault E, Dakos V. 2019 Advancing our understanding of ecological stability. *Ecology letters* **22**, 1349–1356.

[23] Hillebrand H, Langenheder S, Lebret K, Lindström E, Östman Ö, Striebel M. 2018 Decomposing multiple dimensions of stability in global change experiments. *Ecology letters* **21**, 21–30.

[24] Ochoa-Hueso R, Delgado-Baquerizo M, Risch AC, Schrama M, Morriën E, Barmentlo SH, Geisen S, Hannula SE, Resch MC, Snoek BL et al.. 2021 Ecosystem coupling: A unifying framework to understand the functioning and recovery of ecosystems. *One Earth* **4**, 951–966.

[25] Bender EA, Case TJ, Gilpin ME. 1984 Perturbation experiments in community ecology: theory and practice. *Ecology* **65**, 1–13.

[26] Moreno-Mateos D, Alberdi A, Morriën E, van der Putten WH, Rodríguez-Uña A, Montoya D. 2020 The long-term restoration of ecosystem complexity. *Nature Ecology & Evolution* **4**, 676–685.

[27] Thakur MP, Risch AC, van der Putten WH. 2022 Biotic responses to climate extremes in terrestrial ecosystems. *Iscience* **25**.

[28] Martínez-De León G, Marty A, Holmstrup M, Thakur MP. 2024 Population resistance and recovery after an extreme heat event are explained by thermal effects on life-history traits. *Oikos* **2024**, e10023.

[29] Isbell F, Craven D, Connolly J, Loreau M, Schmid B, Beierkuhnlein C, Bezemer TM, Bonin C, Bruelheide H, De Luca E et al.. 2015 Biodiversity increases the resistance of ecosystem productivity to climate extremes. *Nature* **526**, 574–577.

[30] Tohya M, Teramoto K, Watanabe S, Hishinuma T, Shimojima M, Ogawa M, Tada T, Tabe Y, Kirikae T. 2022 Whole-genome sequencing-based re-identification of Pseudomonas putida/fluorescens clinical isolates identified by biochemical bacterial identification systems. *Microbiology Spectrum* **10**, e02491–21.

[31] Sentchilo VS, Perebituk AN, Zehnder AJ, van der Meer JR. 2000 Molecular diversity of plasmids bearing genes that encode toluene and xylene metabolism in Pseudomonas strains isolated from different contaminated sites in Belarus. *Applied and environmental microbiology* **66**, 2842–2852.

[32] Howell C, Stipanovic R. 1979 Control of Rhizoctonia solani on cotton seedlings with Pseudomonas fluorescens and with an antibiotic produced by the bacterium. *Phytopathology* **69**, 480–482.

[33] Batsch M, Guex I, Todorov H, Heiman CM, Vacheron J, Vorholt JA, Keel C, van der Meer JR. 2024 Fragmented micro-growth habitats present opportunities for alternative competitive outcomes. *Nature communications* **15**, 7591.

[34] Péchy-Tarr M, Borel N, Kupferschmied P, Turner V, Binggeli O, Radovanovic D, Maurhofer M, Keel C. 2013 Control and host-dependent activation of insect toxin expression in a root-associated biocontrol pseudomonad. *Environmental microbiology* **15**, 736–750.

[35] Schlechter RO, Jun H, Bernach M, Oso S, Boyd E, Muñoz-Lintz DA, Dobson RC, Remus DM, Remus-Emsermann MN. 2018 Chromatic bacteria–A broad host-range plasmid and chromosomal insertion toolbox for fluorescent protein expression in bacteria. *Frontiers in Microbiology* **9**, 3052.

[36] Mytilinaios I, Salih M, Schofield HK, Lambert RJ. 2012 Growth curve prediction from optical density data. *International journal of food microbiology* **154**, 169–176.

[37] Ghenu AH, Marrec L, Bank C. 2024 Challenges and pitfalls of inferring microbial growth rates from lab cultures. *Frontiers in Ecology and Evolution* **11**, 1313500.

[38] Chen CY, Nace GW, Irwin PL. 2003 A 6× 6 drop plate method for simultaneous colony counting and MPN enumeration of Campylobacter jejuni, Listeria monocytogenes, and Escherichia coli. *Journal of microbiological methods* **55**, 475–479.

[39] Hall BG, Acar H, Nandipati A, Barlow M. 2014 Growth rates made easy. *Molecular biology and evolution* **31**, 232–238.

[40] Mansoury M, Hamed M, Karmustaji R, Al Hannan F, Safrany ST. 2021 The edge effect: A global problem. The trouble with culturing cells in 96-well plates. *Biochemistry and biophysics reports* **26**, 100987.

[41] Elzhov TV, Mullen KM, Spiess AN, Bolker B. 2023 *minpack.lm: R Interface to the Levenberg-Marquardt Nonlinear Least-Squares Algorithm Found in MINPACK, Plus Support for Bounds (version 1.2-4)*. DOI: 10.32614/CRAN.package.minpack.lm.

[42] R Core Team. 2024 *R: A Language and Environment for Statistical Computing*. R Foundation for Statistical Computing Vienna, Austria.

[43] Mira P, Yeh P, Hall BG. 2022 Estimating microbial population data from optical density. *Plos one* **17**, e0276040.

[44] Blazanin M. 2024 gcplyr: an R package for microbial growth curve data analysis. *BMC bioinformatics* **25**, 232.

[45] Oksanen J, Simpson GL, Blanchet FG, Kindt R, Legendre P, Minchin PR, O'Hara R, Solymos P, Stevens MHH, Szoecs E, Wagner H, Barbour M, Bedward M, Bolker B, Borcard D, Carvalho G, Chirico M, De Caceres M, Durand S, Evangelista HBA, FitzJohn R, Friendly M, Furneaux B, Hannigan G, Hill MO, Lahti L, McGlinn D, Ouellette MH, Ribeiro Cunha E, Smith T, Stier A, Ter Braak CJ, Weedon J, Borman T. 2025 *vegan: Community Ecology Package*. DOI: 10.32614/CRAN.package.vegan.

[46] McGillycuddy M, Warton DI, Popovic G, Bolker BM. 2025 Parsimoniously Fitting Large Multivariate Random Effects in glmmTMB. *Journal of Statistical Software* **112**, 1–19. (10.18637/jss.v112.i01)

[47] Hartig F. 2024 *DHARMa: Residual Diagnostics for Hierarchical (Multi-Level / Mixed) Regression Models*. DOI: 10.32614/CRAN.package.DHARMa.

[48] Lüdecke D, Ben-Shachar MS, Patil I, Waggoner P, Makowski D. 2021 performance: An R Package for Assessment, Comparison and Testing of Statistical Models. *Journal of Open Source Software* **6**, 3139. (10.21105/joss.03139)

[49] Torchiano M. 2020 *effsize: Efficient Effect Size Computation.* DOI: 10.32614/CRAN.package.effsize.

[50] Lenth RV. 2025 *emmeans: Estimated Marginal Means, aka Least-Squares Means.* DOI: 10.32614/CRAN.package.emmeans.

[51] Andreani NA, Fasolato L. 2017 *Pseudomonas* and related genera. In *The microbiological quality of food* , pp. 25–59. Elsevier.

[52] Pinto J, Haberkorn C, Franzén M, Tack AJ, Stelkens R. 2025 Fermentative yeast diversity at the northern range limit of their oak tree hosts. *bioRxiv* pp. 2025–01.

[53] Zeigler DR. 2014 The Geobacillus paradox: why is a thermophilic bacterial genus so prevalent on a mesophilic planet?. *Microbiology* **160**, 1–11.

[54] Upton RN, Bach EM, Hofmockel KS. 2019 Spatio-temporal microbial community dynamics within soil aggregates. *Soil Biology and Biochemistry* **132**, 58–68.

[55] Godon JJ, Galès A, Latrille E, Ouichanpagdee P, Seyer JP. 2020 An "overlooked" habitat for thermophilic bacteria: The phyllosphere. *BioDiscovery* **23**.

[56] Thompson LR, Sanders JG, McDonald D, Amir A, Ladau J, Locey KJ, Prill RJ, Tripathi A, Gibbons SM, Ackermann G et al.. 2017 A communal catalogue reveals Earth's multiscale microbial diversity. *Nature* **551**, 457–463.

[57] Concepción-Acevedo J, Weiss HN, Chaudhry WN, Levin BR. 2015 Malthusian parameters as estimators of the fitness of microbes: a cautionary tale about the low side of high throughput. *PloS one* **10**, e0126915.

[58] Balsa-Canto E, Alonso-del Real J, Querol A. 2020 Mixed growth curve data do not suffice to fully characterize the dynamics of mixed cultures. *Proceedings of the National Academy of Sciences* **117**, 811–813.

[59] Dedrick S, Warrier V, Lemon KP, Momeni B. 2023 When does a Lotka-Volterra model represent microbial interactions? Insights from in vitro nasal bacterial communities. *Msystems* **8**, e00757–22.

[60] Schmitz DA, Wechsler T, Mignot I, Kümmerli R. 2024 Predicting bacterial interaction outcomes from monoculture growth and supernatant assays. *ISME communications* **4**, ycae045.

[61] Ramette A, Frapolli M, Fischer-Le Saux M, Gruffaz C, Meyer JM, Défago G, Sutra L, Moënne-Loccoz Y. 2011 Pseudomonas protegens sp. nov., widespread plant-protecting bacteria producing the biocontrol compounds 2, 4-diacetylphloroglucinol and pyoluteorin. *Systematic and applied microbiology* **34**, 180–188.

[62] Vick SH, Fabian BK, Dawson CJ, Foster C, Asher A, Hassan KA, Midgley DJ, Paulsen IT, Tetu SG. 2021 Delving into defence: identifying the Pseudomonas protegens Pf-5 gene suite involved in defence against secreted products of fungal, oomycete and bacterial rhizosphere competitors. *Microbial Genomics* **7**, 000671.

[63] Zhang Q, Kong X, Li S, Chen XJ, Chen XJ. 2020 Antibiotics of Pseudomonas protegens FD6 are essential for biocontrol activity. *Australasian plant pathology* **49**, 307–317.

[64] Vacheron J, Péchy-Tarr M, Brochet S, Heiman CM, Stojiljkovic M, Maurhofer M, Keel C. 2019 T6SS contributes to gut microbiome invasion and killing of an herbivorous pest insect by plant-beneficial Pseudomonas protegens. *The ISME journal* **13**, 1318–1329.

[65] Klappenbach JA, Dunbar JM, Schmidt TM. 2000 rRNA operon copy number reflects ecological strategies of bacteria. *Applied and environmental microbiology* **66**, 1328–1333.

[66] Roller BR, Stoddard SF, Schmidt TM. 2016 Exploiting rRNA operon copy number to investigate bacterial reproductive strategies. *Nature microbiology* **1**, 1–7.

[67] Louca S, Parfrey LW, Doebeli M. 2016 Decoupling function and taxonomy in the global ocean microbiome. *Science* **353**, 1272–1277.

[68] Madin JS, Nielsen DA, Brbic M, Corkrey R, Danko D, Edwards K, Engqvist MK, Fierer N, Geoghegan JL, Gillings M et al.. 2020 A synthesis of bacterial and archaeal phenotypic trait data. *Scientific data* **7**, 170.

[69] Cébron A, Zeghal E, Usseglio-Polatera P, Meyer A, Bauda P, Lemmel F, Leyval C, Maunoury-Danger F. 2021 BactoTraits–A functional trait database to evaluate how natural and man-induced changes influence the assembly of bacterial communities. *Ecological Indicators* **130**, 108047.

[70] Bernardes JP, John U, Woltermann N, Valiadi M, Hermann RJ, Becks L. 2021 The evolution of convex trade-offs enables the transition towards multicellularity. *Nature communications* **12**, 4222.

[71] Hillebrand H, Donohue I, Harpole WS, Hodapp D, Kucera M, Lewandowska AM, Merder J, Montoya JM, Freund JA. 2020 Thresholds for ecological responses to global change do not emerge from empirical data. *Nature Ecology & Evolution* **4**, 1502–1509.